PICTURE OF THE MONTH

Use of Spaceborne Synthetic Aperture Radar Imagery of the Sea Surface in Detecting the Presence and Structure of the Convective Marine Atmospheric Boundary Layer

T. D. SIKORA AND G. S. YOUNG

The Pennsylvania State University, University Park, Pennsylvania

R. C. BEAL

The Johns Hopkins University Applied Physics Laboratory, Laurel, Maryland

J. B. EDSON

Woods Hole Oceanographic Institution, Woods Hole, Massachusetts

3 January 1995 and 14 June 1995

ABSTRACT

Two distinct backscatter regimes are seen on a European remote sensing satellite *ERS-1* C-band (5.6 cm) synthetic aperture radar (SAR) image of the sea surface during a time of fair synoptic-scale weather conditions. One backscatter regime is mottled. In contrast to that, the second backscatter regime is marbled.

The authors hypothesize that the mottled backscatter pattern is a characteristic SAR backscatter pattern linked to the presence of the convective (i.e., statically unstable/convective-eddy containing) marine atmospheric boundary layer (CMABL) and can be used to help determine CMABL structure [convective-eddy type (cellular convection versus longitudinal rolls), eddy wavelength, and CMABL depth (via mixed-layer similarity theory for aspect ratio)]. The hypothesis linking the presence and structure of the CMABL to the mottled backscatter pattern on SAR imagery is validated by analyzing data from a number of sources gathered in the vicinity of the boundary between the mottled and marbled regimes on the SAR image.

1. Introduction

In situ studies of the convective (i.e., statically unstable/convective-eddy containing) marine atmospheric boundary layer (CMABL) have been much more common than remote sensing studies of the CMABL. Numerous field and laboratory experiments have resulted in detailed discussions of CMABL air–sea fluxes (e.g., vertical eddy fluxes of heat, momentum, and moisture) as well as the convective boundary-layer-spanning eddies (BLSEs) [convective updraft (CU)–convective downdraft (CD) couples] that transmit these fluxes through the CMABL (Liu et al. 1979; Lenschow and Stephens 1980; Greenhut and Khalsa 1982; Khalsa and Greenhut 1985; Fairall et al. 1990; Schumann and Moeng 1991; Sikora and Young 1993; among others).

Corresponding author address: Todd D. Sikora, Department of Meteorology, College of Earth and Mineral Sciences, The Pennsylvania State University, 503 Walker Building, University Park, PA 16802-5013.

These studies have revealed that the intensity of air–sea fluxes—as well as the BLSEs through which they are realized—are functions of many variables. To satisfy the need for universal diagnoses of marine atmospheric boundary layer (MABL) flux and eddy statistics, boundary layer similarity relationships have been developed and applied. [See Stull (1988) for an overview of boundary layer similarity theory.] Similarity theory offers a valuable means of relating the statistics of similarity stratified boundary layers through the use of scaling parameters and nondimensional relationships (Lenchow and Stephens 1980; Khalsa and Greenhut 1985; Young 1988; Sikora and Young 1994). Given the resulting similarity formulas and in situ measurements of the scaling parameters [i.e., CMABL depth z_i and the air–sea fluxes], quantitative estimates of the turbulence statistics for a particular CMABL can be calculated.

We will show in the present research that similarity theory can also provide a powerful tool in spaceborne synthetic aperture radar (SAR) remote sensing studies of the CMABL. We will combine traditional boundary layer similarity theory with a new concept we call SAR

similarity (based on pattern recognition) in order to relate backscatter patterns seen on SAR imagery of the sea surface with corresponding CMABL morphology.

Previous spaceborne SAR studies have suggested that kilometer-scale backscatter patterns seen on SAR imagery of the sea surface are manifestations of BLSEs contained within the CMABL (Gerling 1986; Alpers and Brummer 1994; Beal et al. 1994; Nilsson and Tildesley 1995; among others). These kilometer-scale backscatter patterns are thought to be linked to BLSE-induced sea surface roughness patterns composed of waves of centimeter-scale wavelength. These kilometer-scale BLSE-induced sea surface roughness patterns can be detected by SAR in the absence of appreciable non-CMABL sea surface wave forcing phenomena (e.g., heavy slicks that dampen the sea surface roughness field and strong synoptic-scale surface winds that enhance the sea surface roughness field).

Unfortunately, the sea surface SAR imagery acquired in previous studies has not been analyzed with respect to a concurrent, high-resolution boundary layer dataset. For this reason, there has been no hard evidence linking kilometer-scale backscatter patterns on SAR imagery of the sea surface with the presence of MABL convection. In the present research, we will investigate the link between kilometer-scale backscatter patterns on SAR imagery of the sea surface and CMABL morphology using conventional boundary layer theory and supporting meteorological and oceanographic data.

a. Theory

BLSE-induced sea surface roughness patterns result from the mixing down of high-momentum air within the CDs of BLSEs. This transport of high-momentum air into the convective marine atmospheric surface layer (CMASL) is in accordance with parcel mixing theory (Stull 1988) and has been reported in the observational literature (e.g., Wilczak 1984; Khalsa and Greenhut 1985; Schumann and Moeng 1991; Sikora and Young 1993). As the downward-moving, high-momentum air approaches the sea surface, its presence results in a vertical "squeezing" of the CMASL wind profile and, hence, an increase of the CMASL vertical wind shear. This increased wind shear results in enhanced transfer of high-momentum air to the sea surface by CMASL eddies (the feet of BLSEs). As the high-momentum air reaches the sea surface, it spreads out in the form of gusts in the general direction of the boundary-layer mean wind, enhancing sea surface roughness (Watts 1987). The reverse occurs within CUs where vertical "stretching" of the CMASL wind profile reduces the CMASL vertical wind shear. In summary then, the expected footprint of a field of BLSEs in the presence of a boundary layer mean wind is enhanced sea surface roughness beneath and down mean wind of each CD combined with decreased sea surface roughness beneath and down mean wind of each CU.

If there exists such repeatable sea surface roughness signatures that are the footprints of BLSEs, there should also exist repeatable backscatter signatures on SAR imagery of the sea surface beneath the CMABL revealing these footprints. The occurrence of these backscatter signatures on SAR imagery of the sea surface could then be looked upon as being a *characteristic* backscatter pattern depicting the presence of the CMABL.

Numerous conditional sampling and compositing studies of the convective boundary layer (e.g., Khalsa and Greenhut 1985; Young 1988; Schumann and Moeng 1991) and spectral studies of the convective boundary layer (e.g., Kaimal et al. 1972; LeMone 1973; Kaimal et al. 1976; Young 1987) have shown that the occurrence of BLSEs is indeed repeatable, and hence, the occurrence of maxima in CMASL horizontal velocity is a repeatable feature of this phenomenon. In addition, these studies have shown that the horizontal wavelengths of BLSEs as well as peak wavelengths of horizontal velocity spectra are a function of z_i via mixed-layer similarity theory for BLSE aspect ratio (defined as BLSE wavelength divided by z_i). Kaimal et al. (1976) go on to show that the peak wavelength of horizontal velocity spectra does not vary with height from z_i right down to the surface and is approximately $1.5z_i$. These observations lead us to believe that the dominant wavelength of BLSE-induced backscatter signatures from the sea surface, as seen by SAR, can be related to BLSE wavelength and z_i through mixed-layer similarity theory for aspect ratio (discussed in section 3c).

It follows then that in the absence of appreciable non-CMABL sea surface wave forcing phenomena, SAR images of the sea surface depicting characteristic (BLSE induced) backscatter patterns reveal MABLs of similar (convective) stability and can be used to help determine CMABL structure [BLSE type (cellular convection versus longitudinal rolls), BLSE wavelength, and z_i (via mixed-layer similarity theory for aspect ratio)]. These relationships between SAR backscatter patterns from the sea surface and CMABL morphology are what we call SAR similarity.

It should be emphasized here that the idea of SAR similarity in the present research is limited to the CMABL. The concept of SAR similarity is not applied in the present research to the nonconvective (i.e., non-BLSE containing) MABL, as we do not feel there is a single characteristic (i.e., SAR similar) SAR backscatter pattern for the nonconvective MABL (discussed in section 3a). In the following discussion, the references to and use of nonconvective MABL in situ data and corresponding SAR imagery (we use that of the statically stable MABL) are done solely to contrast what is seen there to what is seen for the CMABL.

The concept of SAR similarity is not without precedent. Pattern recognition for feature identification has been used extensively throughout the remote sensing/image analysis community (e.g., Swain et al. 1981; Kandel 1982; Ebert 1987; Key 1990). Putting it in a more meteorological context, the use of SAR similarity in detecting the presence and structure of the CMABL is analogous to the recognition of boundary layer cumulus clouds on a visible satellite image, followed then by an interpretation of the corresponding boundary layer stability and structure (e.g., Miura 1986).

Note, however, that in contrast to Miura's methods, SAR is neither attenuated by clouds nor dependent on clouds. In other words, SAR can "see" through intervening cloud layers and does not require the presence of specific characteristic clouds to be of use in CMABL studies. SAR, therefore, has the advantage of being able to measure the effect of CMABL circulations on the sea surface in both the presence and absence of clouds.

Given all the above, SAR imagery has the potential to provide real-time qualitative and quantitative assessments of MABL static instability and CMABL structure from BLSE-induced backscatter patterns. The concept of SAR similarity can facilitate CMABL research and operational analysis in regions where in situ measurements are unavailable and is equally applicable in cloudy and cloud-free regions.

b. ERS-1 *SAR data*

Figure 1 shows a European remote sensing satellite *ERS-1* C-band (5.6 cm) SAR image of the sea surface taken over the northwestern edge of the Gulf Stream North Wall (GSNW), just east of the North Carolina coast (referred to as the imaged area). The image is from *ERS-1* orbit 10 047 at 1538 UTC 17 June 1993. The SAR image, composed of portions of two adjacent 100-km-square frames, is approximately 100 km in the cross-track direction by 140 km in the along-track direction, with a pixel size of 100 m. In the cross-track direction, a systematic trend resulting from the radar antenna pattern has been removed, and the resulting radar backscatter variations have been linearly expanded to use the full dynamic range of display. Using the frame corner coordinates as guides, a reference grid (identical to that used in Figs. 4–7) has been superimposed on the image.

c. Goals

Within Fig. 1, areas of enhanced sea surface roughness appear as lighter shaded pixels, while darker pixels denote a more quiescent sea surface. Two distinct backscatter regimes can be seen in Fig. 1. The first is a mottled backscatter pattern seen throughout the southeast portion of the image. The second is a marbled backscatter pattern seen throughout the northwest portion of the image. The border between these two backscatter regimes lies approximately from 35.45°N, 74.95°W to 36.15°N, 73.75°W. It will be shown later that this border lies along the GSNW.

We hypothesize that the mottled backscatter pattern seen in Fig. 1 is a characteristic SAR backscatter pattern linked to the presence of the CMABL and can be used to help determine CMABL structure in the presence of fair synoptic-scale weather conditions (e.g., calm to light surface winds, precipitation free). The logic behind the development of our hypothesis linking the presence and structure of the CMABL to the mottles was described above in section 1a using CMASL air–sea momentum flux/BLSE footprint arguments. In the following sections, our hypothesis is given credence by demonstrating the occurrence of mottles in previous SAR studies of the sea surface. Our hypothesis is validated by analyzing National Climatic Data Center (NCDC), National Meteorological Center (NMC), National Oceanic and Atmospheric Administration (NOAA), and National Weather Service (NWS) analysis products, as well as data taken during experiment High-Resolution 2 (HI-RES 2), from the mottled and marbled backscatter regimes in the vicinity of the GSNW. For a review of HI-RES 2, see Thompson et al. (1994).

2. Meteorological conditions

Synoptic-scale meteorological conditions in the imaged area were uniformly fair at the time of the *ERS-1* overpass. Figure 2 shows the 1500 UTC 17 June 1993 surface analysis generated at NCDC. A stationary front extends from western North Carolina northeastward to a weak low pressure wave near Virginia Beach, Virginia. From the low pressure wave, the stationary front continues east-southeastward over the Atlantic Ocean. The imaged area was therefore located within a uniform, relatively warm air mass south of this front. This situation is consistent with HI-RES 2 shipboard-measured mean wind speeds of 4–5 kt from the west-southwest during this period.

NMC upper-air analyses from 1200 UTC 17 June 1993 (not shown) showed the imaged area to be just east of a large upper-air ridge. At Cape Hatteras (HAT), 850-mb winds were 10 kt from the northeast, 700-mb winds were 10 kt from the north, and 500-mb winds were 10 kt from the northwest.

Inspection of the NMC surface analyses between 1200 and 1800 UTC (not shown) indicated no precipitation over eastern North Carolina or adjacent coastal waters. In addition, NWS radar composites from 1235 UTC 17 June 1993 through 1835 UTC 17 June 1993 (not shown) showed the imaged area, as well as all of eastern North Carolina, to be free of precipitation. Given all the above information, it can be concluded that the imaged area was located within a region of undisturbed weather on the synoptic scale. Thus, the observed variation in SAR backscatter pattern across the imaged area is not of synoptic origin.

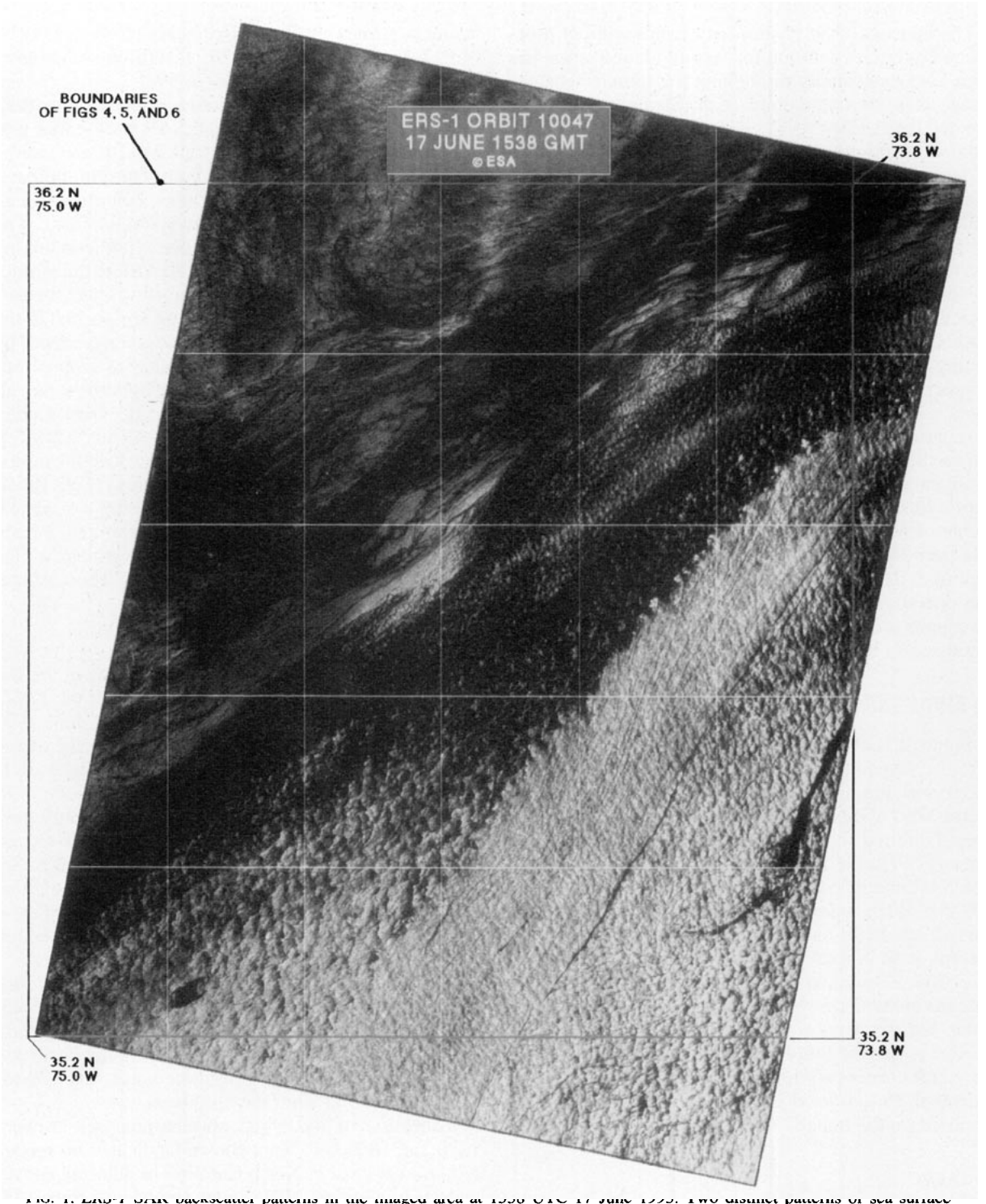

FIG. 1. ERS-1 SAR backscatter patterns in the imaged area at 1538 UTC 17 June 1993. Two distinct patterns of sea surface roughness are detected by SAR within the imaged area. The first is a mottled backscatter pattern throughout the southeast portion of the image. The second is a marbled backscatter pattern throughout the northwest portion of the image.

While no synoptic-scale disturbed weather system was depicted on NMC analyses over the imaged area, observation notes from meteorological personnel aboard the R/V *Columbus Iselin,* participating in experiment HI-RES 2 within the imaged area, report an atmospheric mesofront in the vicinity of the GSNW.

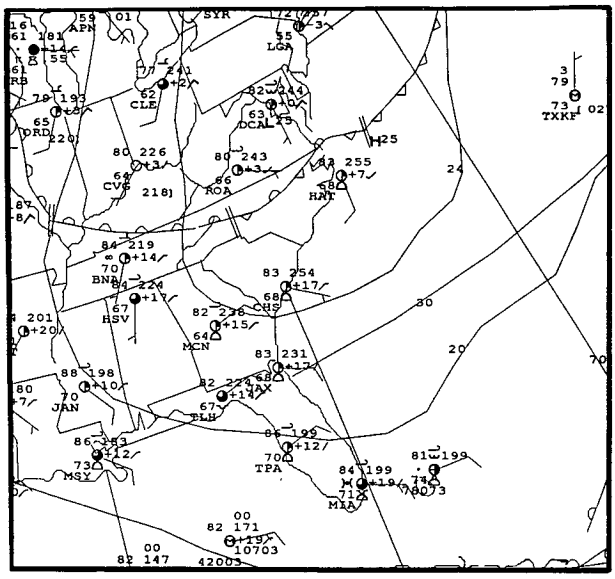

FIG. 2. Synoptic surface analysis for 1500 UTC 17 June 1993.

Clear and calm conditions were reported on the nearshore side of this mesofront, while light winds and boundary layer cumulus clouds were observed on the offshore, Sargasso Seaside. The response of the *ERS-1* SAR backscatter in the vicinity this atmospheric–oceanic front will be the emphasis of the following discussion.

3. Discussion

a. Boundary layer stability

As discussed in section 1, we assert that the mottles seen on the southeast portion of Fig. 1 result from kilometer-scale modulations of the capillary (centimeter scale) sea surface wave field caused by air–sea momentum flux patterns associated with sea surface footprints of BLSEs. These wave patterns are akin to cat's-paws rippling across a pond during conditions of strong turbulence, such as those presented by Dorman and Mollo-Christensen (1973). The hypothesized convectively induced mottles seen in the present research, however, exhibit scales on the order of z_i as opposed to Dorman and Mollo-Christensen's shear-driven cat's-paws that have scales on order of meters.

Additional examples of this type of mottled backscatter pattern have been seen in numerous SAR images of the sea surface, such as that seen in Fig. 3a provided by Beal et al. (1994). The literature provides ample examples of this characteristic backscatter pattern from many different SAR platforms. Gerling (1986) uses Seasat SAR to show such kilometer-scale variations in the radar backscatter. Beal et al. (1994) present a mosaic of backscatter patterns seen by *ERS-1* SAR, including the characteristic mottled backscatter pattern. Trokhimovsky et al. (1994) reported JPL and *ERS-1* C-band SAR detection of the characteristic mottled pattern. Nilsson and Tildesley (1995) also make reference to the mottled backscatter pattern seen on *ERS-1* SAR imagery. These observations demonstrate the characteristic nature of mottles on SAR imagery of the sea surface and therefore lend credence the concept of SAR similarity.

In contrast to the mottled backscatter pattern, it is believed that the marbled backscatter pattern, evident on the region encompassing the northwest portion of Fig. 1, is related to the occurrence of a statically stable MABL in that region. Additional examples of marbling on SAR imagery can be seen in Fig. 3b (provided by Beal et al. 1994) as well as in Nilsson and Tildesley (1995). This marbling most likely occurs due to the combination of calm surface winds in a statically stable MABL and the presence of sea surface surfactant slicks (SSSS) (Nilsson and Tildesley 1995). Therefore, this marbling is probably not a characteristic SAR backscatter pattern depicting the effect of the structure of the statically stable MABL on the sea surface in the presence of fair synoptic-scale weather conditions. Rather, it is a manifestation of several different small-scale oceanic and large-scale atmospheric factors. It is beyond the scope of this paper to thoroughly discuss the detection and morphology of SSSS and the marbled backscatter pattern on SAR imagery. For further review of this topic, the reader is directed to Najjar (1992), Huhnerfuss et al. (1994), and Nilsson and Tildesley (1995).

As stated earlier, the sea surface SAR imagery acquired in previous studies have not been analyzed with respect to a concurrent, high-resolution boundary layer dataset. For this reason, there has been no hard evidence linking the mottles seen in SAR imagery of the sea surface to MABL convection. In the present research, our hypothesis linking the existence of mottled backscatter patterns on SAR imagery of the sea surface to the presence and structure of CMABLs will be val-

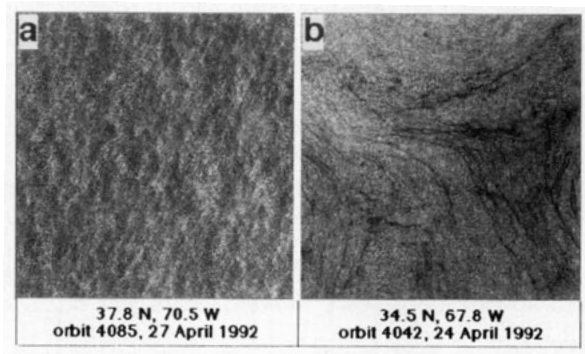

FIG. 3. Excerpts of *ERS-1* SAR imagery provided by Beal et al. (1994) along with appropriate center coordinates, orbit number, and date showing (a) a mottled backscatter pattern and (b) a marbled backscatter pattern. Horizontal dimensions are 10 km.

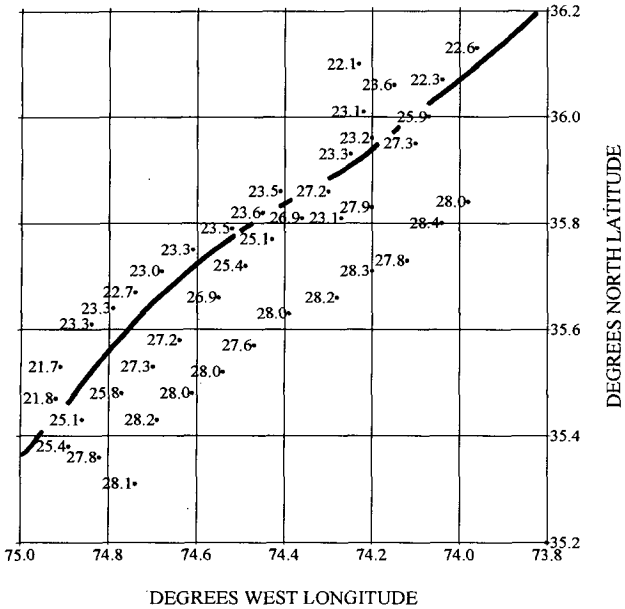

FIG. 4. Map of 10-min mean SSTs (°C) taken aboard the R/Vs *Columbus Iselin* and *Bartlett* from 0002 UTC 16 June 1993 through 2236 UTC 18 June 1993. The GSNW is depicted by the dark solid line. Note the wonderful alignment of the GSNW with the marble–mottle demarcation seen in Fig. 1.

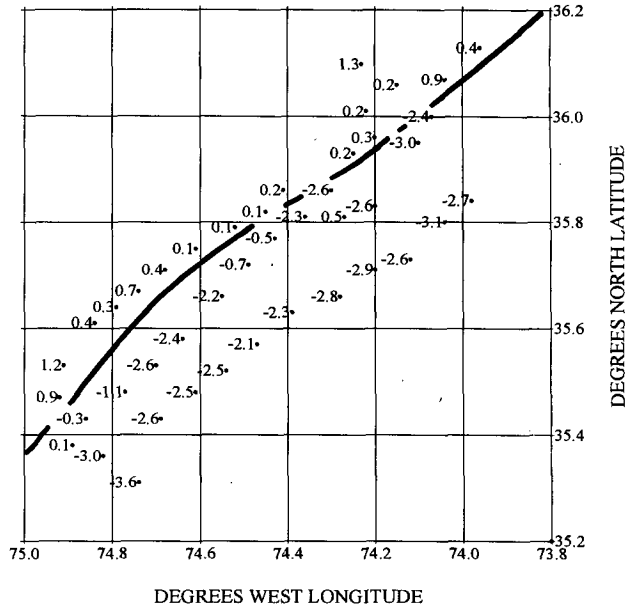

FIG. 5. Same as in Fig. 4 but for T_{air} at 10 m $- T_{sea}$ (°C). Note that negative values are seen to the east of the GSNW, indicative of a CMABL. In contrast, positive values are found to the west of the GSNW indicative of a statically stable MABL.

idated using such a dataset composed of observations from a number of sources.

Inspection of the NOAA oceanographic features analysis (OFA) for 17 June 1993 (not shown) indicated that the border between the two backscatter regimes seen in Fig. 1 lies along the GSNW. The OFA showed sea surface temperatures (SSTs) in the imaged area to be in the range of 22°–24°C on the western side of the GSNW and 27°–28°C on the eastern side. This observation suggests that MABL convection was more likely to the east of the GSNW rather than to the west of the GSNW. To confirm or deny the existence of a CMABL on either side of the GSNW, a high-resolution MABL dataset needs to be employed, such as that taken aboard the R/Vs *Columbus Iselin* and *Bartlett* during experiment HI-RES 2.

In the following discussion, most in situ ship data presented from HI-RES 2 to the south and east of the GSNW, over the mottled regime, are from the R/V *Columbus Iselin.* Most in situ ship data presented from HI-RES 2 to the north and west of the GSNW, over the marbled regime, are from the R/V *Bartlett.* All in situ ship data presented from HI-RES 2 are 10-min means.

Figure 4 shows a map of 10-min mean SSTs (°C) taken aboard the R/Vs *Columbus Iselin* and *Bartlett* from 0002 UTC 16 June 1993 through 2236 UTC 18 June 1993. The GSNW, depicted as a dark solid line in Fig. 4, aligns rather well with the mottle–marble interregime border seen in Fig. 1. Figure 5 is a corresponding map of air–sea temperature difference (°C) (T_{air} at 10 m $- T_{sea}$). As is expected from the hypothetical interpretation of the SAR image, negative values of air–sea temperature difference are generally seen to the east of the GSNW, indicative of a CMABL.

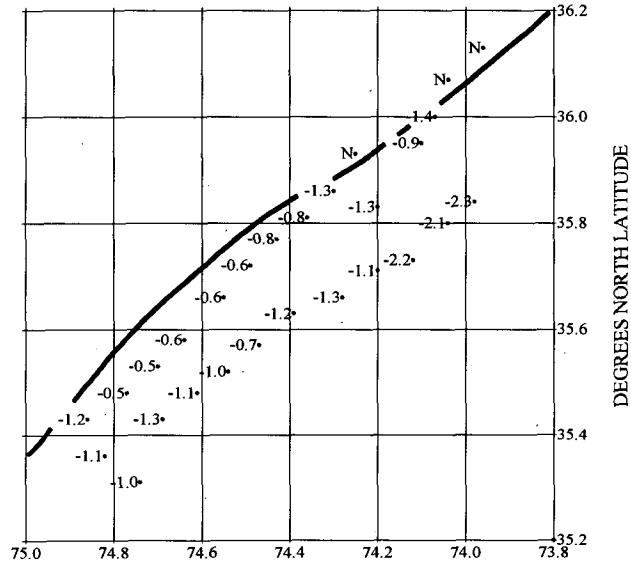

FIG. 6. Map of ratios of instrument height (z = 10 m) to Obukhov length L (m) (z/L) corresponding to R/V *Columbus Iselin* datapoint locations in Figs. 4 and 5. The GSNW is depicted by the dark solid line. Static instability is found to the east of the GSNW.

In contrast, positive values are observed to the west of the GSNW, indicative of a statically stable MABL.

Another measure of MABL static stability can be determined using Monin–Obukhov similarity. [See Stull (1988) for a review of Monin–Obukhov similarity theory.] Figure 6 shows ratios of instrument height (z = 10 m) versus Obukhov length L (m):

$$\frac{z}{L} = \frac{-zkg\overline{(w'\theta_v')_s}}{\overline{\theta_v}u_*^3}, \qquad (1)$$

corresponding to *Columbus Iselin* data point locations in Figs. 4 and 5. (Insufficient data prevented the calculation of z/L at Bartlett datapoint locations.) In (1), k is the von Kármán constant (0.40), g is the acceleration due to gravity (9.8 m s^{-2}), $\overline{(w'\theta_v')_s}$ is the air–sea buoyancy flux (m s^{-1} K), $\overline{\theta_v}$ is the average virtual potential temperature (K), and u_* is the friction velocity (m s^{-1}).

It is important to note here that the fluxes from the R/V *Columbus Iselin* were computed using the direct covariance method (Hare et al. 1992). Therefore, the sign of z/L is determined by the fluxes themselves and not by the sign of the air–sea temperature difference, as would be the case with the bulk and inertial dissipation methods. Thus, the z/L map provides a stability field independent of the air–sea temperature difference map. The results seen in Fig. 6 for z/L show that static instability was generally observed to increase (increasing negative values of z/L) the farther east of the GSNW the *Columbus Iselin* sailed. Neutral stability (i.e., zero buoyancy flux), denoted by "N" on Fig. 6, is seen in a few locations adjacent to the front.

The above in situ observations, combined with Monin–Obukhov similarity theory, support our hypothesis linking boundary layer convection with the observed mottled SAR backscatter pattern. Over warm waters east of the GSNW, where the mottled backscatter pattern appears on the SAR imagery, a CMABL is observed. In contrast, over cool waters to the west of the GSNW, where marbling appears on the SAR imagery, a statically stable MABL is observed. As stated earlier, it is believed from previous studies that the marbling seen beneath the statically stable MABL results from the combination of calm surface winds associated with the statically stable MABL and the presence of SSSS (Najjar 1992; Huhnerfuss et al. 1994; Nilsson and Tildesley 1995).

The close spatial correspondence between the mottled/marbled SAR regimes and the statically unstable/stable MABL stability regimes in the present research, combined with the characteristic nature of mottles as seen in previous SAR studies of the sea surface, supports the use of SAR similarity. [That is, we believe there is a one-to-one match between the occurrence of the characteristic SAR backscatter pattern at a point (mottled) and the occurrence of the corresponding atmospheric phenomena present at that point (CMABL).] Admittedly, though, we do find in Fig. 1 a portion of the in situ data containing the CMABL regime that does not contain mottles. This portion lies directly adjacent to the GSNW near its southwestern-most extent in Fig. 1. An explanation of this phenomenon is given in section 3c.

b. BLSE type: Cells or rolls

Within convective boundary layers, two distinct types of boundary layer circulation have been noted in the literature, cellular convection and longitudinal rolls (e.g., Woodcock 1975; Deardorff 1976; Brown 1980; Miura 1986; Alpers and Brummer 1994). The occurrence of one type or the other is dependent on the degree of boundary layer wind shear and instability (Haack and Shirer 1992). Unfortunately, accurate MABL wind data within the imaged area for 17 June is lacking. This shortcoming of the available soundings hinders the use of mixed-layer similarity theory to diagnose the type of BLSE present within the mottled regime of Fig. 1. Observational results presented by Woodcock (1975) and verified theoretically by Deardorff (1976) can, however, be used to diagnose the type of BLSE from just the air–sea temperature difference and the wind speed at 10 m using surface-layer similarity.

Inspection of the *Columbus Iselin* in situ dataset reveals that the wind speed at 10 m above sea level never exceeded 6 m s^{-1} during 17 June 1993, while the air–sea temperature differences on the Sargasso Seaside of the GSNW ranged up to −3.6°C. Using these values as inputs into the nomogram given by Woodcock (1975) and Deardorff (1976) (not shown) suggests that cellular convection rather than longitudinal rolls are dominant within at least that part of the mottled regime of Fig. 1 where in situ data are available. The agreement of this result with the observed cellular shape and intermittent distribution of the mottles leads us to believe that the mottled SAR backscatter pattern of the sea surface is the characteristic backscatter pattern of CMABL cellular convection. This cellular backscatter pattern is in contrast to the linear banded *ERS-1* SAR backscatter pattern observed in Alpers and Brummer (1994) and thought to be the result of longitudinal rolls.

When viewing Fig. 1, occasional linear southwest–northeast streaks are apparent far to the southeast of the GSNW, out of the area in Figs. 4–6 containing in situ data. These streaks may be the result of linear stretched SSSS or they may be the SAR backscatter pattern of boundary layer roll vortices. Future research will include the detailed analysis of in situ atmospheric and oceanographic data within this region in an effort to explain the streaks.

c. Aspect ratio

Recall from section 1a that numerous boundary layer compositing and spectral studies have shown that the

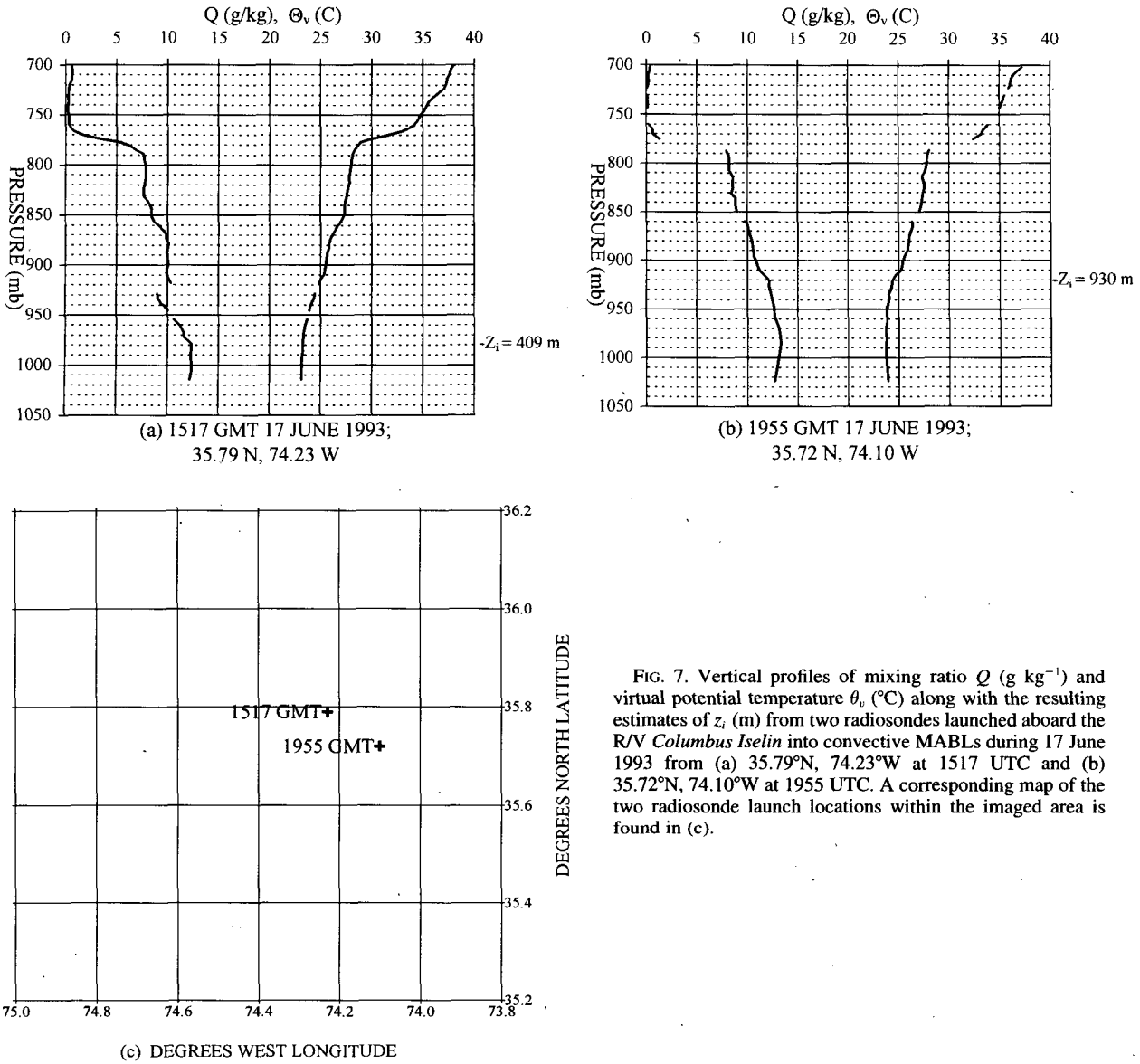

FIG. 7. Vertical profiles of mixing ratio Q (g kg^{-1}) and virtual potential temperature θ_v (°C) along with the resulting estimates of z_i (m) from two radiosondes launched aboard the R/V *Columbus Iselin* into convective MABLs during 17 June 1993 from (a) 35.79°N, 74.23°W at 1517 UTC and (b) 35.72°N, 74.10°W at 1955 UTC. A corresponding map of the two radiosonde launch locations within the imaged area is found in (c).

horizontal wavelength of a BLSE is a function of z_i. Mixed-layer similarity relationships for BLSE aspect ratio have therefore been developed and applied to universally scale BLSE wavelength to z_i (e.g., Miura 1986).

Young (1988) shows that the dominant horizontal wavelength of BLSEs in the convective boundary layer is about $1.5z_i$. This aspect ratio value of 1.5 matches well with other studies. Recall from section 1a that Kaimal et al. (1976) show that the peak wavelength of horizontal velocity spectra does not vary with height from z_i right down to the surface and is also approximately $1.5z_i$. Recall also the arguments of section 1a linking mottles to the footprints of BLSEs, which lead us to believe that the wavelength of the mottles as seen by SAR can be equated to BLSE wavelength. This hypothesized relationship will now be substantiated through a comparison of the ratio of mottle wavelength to z_i versus the similarity theory value for the ratio of BLSE wavelength to z_i.

Following our logic given in section 1a, a mottle wavelength is taken to be the distance from the up-mean-wind backscatter edge of one bright mottle to the corresponding edge of the next down-mean-wind bright mottle. A sample of 50 mottle wavelengths were measured from the in situ data containing region of Fig. 1. The measurements were made by hand using a divider. The average measured wavelength of a mottle is 1.33 km with a standard deviation of 0.5 km.

To evaluate z_i in the mottled portion of the in situ data-containing region, radiosonde profiles are employed. Figures 7a,b show the two radiosonde profiles

of mixing ratio Q (g kg^{-1}) and virtual potential temperature θ_v (°C), along with the resulting estimates of z_i (m). Figure 7c shows the corresponding radiosonde launch locations from the R/V *Columbus Iselin* within the imaged area. The average z_i taken from the two soundings is 670 m.

Therefore, the average mottle aspect ratio (mottle wavelength divided by z_i) seen in the present research is 1.98 plus or minus 0.5. This value compares well with the previously mentioned studies of Kaimal et al. (1976) and Young (1988) for the BLSE aspect ratio. Thus, it appears that the average wavelength of the mottles does indeed approximate the average wavelength of the corresponding BLSEs.

Note also that in Fig. 1 the scale of the BLSE-induced mottles increases to the south and east of the GSNW. Given the above aspect ratio argument, this scale gradient would lead one to believe that z_i also increases to the south and east of the GSNW. The soundings in Figs. 7a,b support this SAR-based diagnosis. CMABL depth does indeed increase to the south and east of the GSNW. This relationship between the geographical trends in z_i and mottle wavelength lends further credence to our hypothesis that the mottled backscatter pattern does result from BLSEs that scale with z_i.

The above given relationship between mottle wavelength, BLSE wavelength, and z_i also helps explain why no mottles are seen in one portion of the in situ data containing the CMABL regime of Fig. 1. This portion lies directly adjacent to the GSNW near its southwestern-most extent in Fig. 1. Presumably, z_i in this marginal area is not deep enough to support BLSEs capable of reaching the elevation necessary to mix down momentum of enough magnitude to cause SAR-detectable sea surface roughness patterns (as discussed in section 1a).

Given all the above, we feel that mottle wavelengths do indeed correspond to BLSE wavelengths. Thus, for operational analyses, the above given SAR similarity procedure could be reversed to obtain an estimate of z_i from SAR imagery using this value of the mottle aspect ratio. Future research will include more sophisticated spectral methods for obtaining estimates of mottle wavelength and, thus, z_i.

4. Conclusions

Sea surface manifestations of CMABL cellular convection are evident on the *ERS-1* SAR image seen in Fig. 1. In the presence of fair synoptic-scale weather conditions, CMASL winds flowing out of CDs and into CUs modulate air–sea momentum flux patterns that in turn force SAR-detectable roughness patterns in the sea surface wave field. These kilometer-scale modulations of the capillary sea surface wave state appear as a characteristic mottled backscatter pattern as demonstrated by its detection in numerous other SAR studies of the sea surface (e.g., Gerling 1986; Beal et al. 1994; Trokhimovsky et al. 1994; Nilsson and Tildesley 1995). These previous observations combined with what has been presented in the present research demonstrate the characteristic nature of mottles on SAR imagery of the sea surface, thereby lending credence to the concept of SAR similarity.

In contrast, a cool sea surface beneath a statically stable MABL is denoted by a marbled backscatter pattern on our SAR image. The marbling is most likely associated with nearly calm surface winds in the statically stable MABL and the presence of sea surface surfactant slicks (Najjar 1992; Huhnerfuss et al. 1994, and Nilsson and Tildesley 1995).

The occurrence and nonoccurrence of the characteristic, SAR-similar, mottled backscatter pattern on SAR imagery of the sea surface allows one to infer the presence of the CMABL and BLSE circulation type. Moreover, CMABL depth can be related to the observed mottle wavelength using mixed-layer similarity theory for BLSE aspect ratio. These results can be applied to the nowcasting of oceanic fronts and stability-related radar ducting phenomena and should be of interest to the air–sea interaction research community (Sweet et al. 1981; Wai and Stage 1989; Doyle and Warner 1990; Sublette and Young 1994).

Future research will include spectral and textural classification of SAR imagery, along with detailed statistical ground truthing, in order to obtain quantitative descriptions of sea surface stress patterns and the CMASL wind field, induced by differing scales of convection as seen by SAR. In addition, initial comparisons of the BLSE-induced SAR backscatter pattern to sea surface stress patterns derived from a nonlinear dynamical model (Shirer et al. 1995) are heartening. Close collaboration between the image analysis and model research will continue.

Acknowledgments. The authors would like to thank M. S. Sublette and J. E. Hare for their help with data acquisition. The authors would also like to acknowledge the European Space Agency for supplying the SAR image. The authors would finally like to thank the anonymous reviewers for their very helpful comments. The research reported in this work was funded by the Office of Naval Research under Grants N00014-90-J-4012 and N00014-92-J-1585.

REFERENCES

Alpers, W., and B. Brummer, 1994: Atmospheric boundary layer rolls observed by the synthetic aperture radar aboard the ERS-1 satellite. *J. Geophys. Res.*, **99,** 12 613–12 621.

Beal, R., V. Kudryavtsev, D. Thompson, S. Grodsky, D. Tilley, and V. Dulov, 1994: Large and small scale circulation signatures of the ERS-1 SAR over the Gulf Stream. *Proc. Second ERS-1 Symp.-Space at the Service of our Environment,* Hamburg, Germany, ESA SP-361, 547–552.

Brown, R. A., 1980: Longitudinal instabilities and secondary flows in the planetary boundary layer: A review. *Rev. Geophys. Space Phys.*, **18,** 683–697.

Deardorff, J. W., 1976: Discussion of 'Thermals over the sea and gull flight behavior' by A. H. Woodcock. *Bound.-Layer Meteor.,* **10,** 241–246.

Dorman, C. E., and E. Mollo-Christensen, 1973: Observation of the structure on moving gust patterns over a water surface (''cat's paws''). *J. Phys. Oceanogr.,* **3,** 120–132.

Doyle, J. D., and T. T. Warner, 1990: Mesoscale coastal processes during GALE IOP 2. *Mon. Wea. Rev.,* **118,** 283–308.

Ebert, E., 1987: A pattern recognition technique for distinguishing surface and cloud types in the polar regions. *J. Climate Appl. Meteor.,* **26,** 1412–1427.

Fairall, C. W., J. B. Edson, S. E. Larsen, and P. G. Mestayer, 1990: Inertial-dissipation air–sea flux measurements: A prototype system using realtime spectral computations. *J. Atmos. Oceanic Technol.,* **7,** 425–453.

Gerling, T. W., 1986: Structure of the surface wind field from the Seasat SAR. *J. Geophys. Res.,* **91,** 2308–2320.

Greenhut, G. K., and S. J. S. Khalsa, 1982: Updraft and downdraft events in the atmospheric boundary layer over the equatorial Pacific Ocean. *J. Atmos. Sci.,* **39,** 1803–1818.

Haack, T., and H. N. Shirer, 1992: Mixed convective-dynamic roll vortices and their effects on initial wind and temperature profiles. *J. Atmos. Sci.,* **49,** 1181–1201.

Hare, J. E., J. B. Edson, E. J. Bock, and C. W. Fairall, 1992: Progress on direct covariance measurements of air–sea fluxes from ships and buoys. Preprints, *10th Symp. on Turbulence and Diffusion,* Portland, OR, Amer. Meteor. Soc., 281–284.

Huhnerfuss, H., A. Gericke, W. Alpers, R. Theis, V. Wismann, and P. A. Lange, 1994: Classification of sea slicks by multifrequency radar techniques: New chemical insights and their geophysical implications. *J. Geophys. Res.,* **99,** 9835–9845.

Kaimal, J. C., J. C. Wyngaard, D. A. Haugen, O. R. Cote, Y. Izumi, S. J. Caughey, and C. J. Readings, 1976: Turbulence structure in the convective boundary layer. *J. Atmos. Sci.,* **33,** 2152–2169.

——, ——, Y. Izumi, and O. R. Cote, 1972: Spectral characteristics of surface-layer turbulence. *Quart. J. Roy. Meteor. Soc.,* **98,** 563–589.

Kandel, A., 1982: *Fuzzy Techniques in Pattern Recognition.* Wiley, 356 pp.

Key, J., 1990: Cloud cover analysis with arctic advanced very high resolution radiometer data. Part 2: Classification with spectral and textural measures. *J. Geophys. Res.,* **95,** 7661–7675.

Khalsa, S. J. S., and G. K. Greenhut, 1985: Conditional sampling of updrafts and downdrafts in the marine atmospheric boundary layer. *J. Atmos. Sci.,* **42,** 2550–2562.

LeMone, M. A., 1973: The structure and dynamics of horizontal roll vortices in the planetary boundary layer. *J. Atmos. Sci.,* **30,** 1077–1091.

Lenschow, D. H., and P. L. Stephens, 1980: The role of thermals in the convective boundary layer. *Bound.-Layer Meteor.,* **19,** 509–532.

Liu, W. T., K. B. Katsaros, and J. A. Businger, 1979: Bulk parameterization of air–sea exchanges of heat and water vapor including the molecular constraints at the interface. *J. Atmos. Sci.,* **36,** 1722–1735.

Miura, Y., 1986: Aspect ratios of longitudinal rolls and convection cells observed during cold air outbreaks. *J. Atmos. Sci.,* **43,** 26–39.

Najjar, R. G., 1992: Marine biogeochemistry. *Climate System Modeling,* K. E. Trenberth, Ed., Cambridge University Press, 241–283.

Nilsson, C. S., and P. C. Tildesley, 1995: Imaging of oceanic features by ERS 1 synthetic aperture radar. *J. Geophys. Res.,* **100,** 953–967.

Schumann, U., and C.-H. Moeng, 1991: Plume fluxes in clear and cloudy convective boundary layers. *J. Atmos. Sci.,* **48,** 1746–1757.

Shirer, H. N., L. V. Zuccarello, P. J. Bromfield, B. A. Lambert, and R. Wells, 1995: Sea surface stress variability caused by kilometer-scale boundary layer circulations. Preprints, *11th Symp. on Boundary Layers and Turbulence,* Charlotte, NC, Amer. Meteor. Soc., 76–79.

Sikora, T. D., and G. S. Young, 1993: Observations of planview flux patterns within convective structures of the marine atmospheric surface layer. *Bound.-Layer Meteor.,* **65,** 273–288.

——, and ——, 1994: Observations and applications of the horizontal perturbation wind field within convective structures of the marine atmospheric surface layer. *Bound.-Layer Meteor.,* **68,** 419–426.

Stull, R. B., 1988: *An Introduction to Boundary Layer Meteorology.* Kluwer Academic Publishers, 666 pp.

Sublette, M. S., and G. S. Young, 1994: An analysis of the Gulf Stream atmospheric front during the summer season. Preprints, *Sixth Conf. on Mesoscale Processes,* Portland, OR, Amer. Meteor. Soc., 258–261.

Swain, P. H., S. B. Vardeman, and J. C. Tilton, 1981: Contextual classification of multispectral image data. *Pattern Recognit.,* **13,** 429–441.

Sweet, W., R. Fett, J. Kerling, and P. La Violette, 1981: Air–sea interaction effects in the lower troposphere across the north wall of the Gulf Stream. *Mon. Wea. Rev.,* **109,** 1042–1052.

Thompson, D. R., J. C. Graber, and R. E. Carande, 1994: Measurements of ocean currents with SAR interferometry and HF radar. *Int. Geoscience and Remote Sensing Symp. 94,* Pasadena, CA, IEEE 2020–2022.

Trokhimovsky, Y. G., V. Yakovlev, R. D. Chapman, and D. R. Thompson, 1994: The coherence of wind and radar data obtained during the joint US–Russia Internal Wave Experiment. *Int. Geoscience and Remote Sensing Symp. 94,* Pasadena, CA, IEEE 802–804.

Wai, M. M.-K., and S. A. Stage, 1989: Dynamic analysis of marine atmospheric boundary layer structure near the Gulf Stream oceanic front. *Quart. J. Roy. Meteor. Soc.,* **115,** 29–44.

Watts, A., 1987: *Wind and Sailing Boats, the Structure and Behavior of the Wind as it Affects Sailing Craft.* David and Charles, 224 pp.

Wilczak, J. M., 1984: Large-scale eddies in the unstably stratified atmospheric surface layer. Part I: Velocity and temperature structure. *J. Atmos. Sci.,* **41,** 3537–3550.

Woodcock, A. H., 1975: Thermals over the sea and gull flight behavior. *Bound.-Layer Meteor.,* **9,** 63–68.

Young, G. S., 1987: Mixed layer spectra from aircraft measurements. *J. Atmos. Sci.,* **44,** 1251–1256.

——, 1988: Turbulence structure of the convective boundary layer. Part II: Phoenix 78 aircraft observations of thermals and their environment. *J. Atmos. Sci.,* **45,** 727–735.